frontiers | Frontiers in Earth Science

TYPE Review
PUBLISHED 25 September 2023
DOI 10.3389/feart.2023.1149020



OPEN ACCESS

EDITED BY
Severine Moune,
UMR6524 Laboratoire Magmas et Volcans (LMV), France

REVIEWED BY
Madison Myers,
Montana State University, United States
Roberto Moretti,
UMR7154 Institut de Physique du Globe de Paris (IPGP), France

*CORRESPONDENCE
Maylis Dupont de Dinechin,
maylis.dupont_de_dinechin@sorbonne-universite.fr
Hélène Balcone-Boissard,
helene.balcone_boissard@sorbonne-universite.fr
Caroline Martel,
caroline.martel@cnrs-orleans.fr
Monika Rusiecka,
monika.k.rusiecka@gmail.com

†These authors have contributed equally to this work and share first authorship

RECEIVED 20 January 2023
ACCEPTED 13 September 2023
PUBLISHED 25 September 2023

CITATION
Dupont de Dinechin M, Balcone-Boissard H, Martel C and Rusiecka M (2023), Lithium in felsic magmas: a volcanological perspective. *Front. Earth Sci.* 11:1149020. doi: 10.3389/feart.2023.1149020



# Lithium in felsic magmas: a volcanological perspective

Maylis Dupont de Dinechin[1,2*†], Hélène Balcone-Boissard[1*†], Caroline Martel[2*†] and Monika Rusiecka[2*†]

[1]Sorbonne Université, CNRS, Institut des Sciences de la Terre de Paris (ISTeP), Paris, France, [2]Université d'Orléans, CNRS, BRGM, Institut des Sciences de la Terre d'Orléans (ISTO), Orleans, France

Volcanic eruptions are unpredictable phenomena that pose a challenge to crisis management, owing to the fact that contrasted eruptive styles (explosive versus effusive) exhibited at the surface depend on unobservable deep processes occurring in the reservoir and the volcanic conduit. Constricting the behaviour of magma during ascent, and the degassing in particular, allows for a clearer understanding of the relationships between petrological and volcano monitoring signals, and hence a better description of the volcanic hazard. To this aim, lithium (Li) has been used to track magmatic and post-eruptive processes, as a geospeedometer for processes operating on short time scales due to its high mobility in silicate melts and crystals. Yet, the accurate use of Li to assess syn- and post-eruptive processes still lack complete dataset. We propose a review of our current knowledge on Li behavior, with an emphasis on felsic (andesitic to rhyolitic) magmas whose explosive behavior during volcanic eruptions is still poorly understood. We present current knowledge regarding the Li concentration and isotopic compositions, intracrystalline diffusion, and crystal-melt-fluid partition coefficients discovered in felsic magmas and primary crystals. We describe difficulties in interpreting Li data to investigate the differentiation, degassing, ascent rate, volatile fluxing, and cooling of magmas. Finally, we suggest future directions for expanding our understanding of Li behavior.

KEYWORDS

**lithium, degassing, geospeedometer, diffusion, plagioclase, brines, partition coefficient**

## 1 Introduction

Lithium, along with helium and hydrogen, was one of the first elements created during big-bang nucleosynthesis, but it was not known until it was discovered by J.A. Arfwedson in phyllosilicate (petalite, $LiAlSi_4O_{10}$) minerals in 1817 (Berzelius, 1817). Since its discovery, Li has primarily been regarded as an economic resource exploited for industrial purposes (e.g., battery component, ceramics, glassware, etc.) and medicine. Recently, the global concern about energy transition has boosted research on Li as a means of economic decarbonation (IEA, 2021). In nature, Li mostly concentrates in brines (due to Li solubility in water as salts with inorganic anions and hydroxides as LiOH; Munk et al., 2016), clays, and enriched granitic pegmatites. Li concentration in felsic rocks is a direct consequence of Li incompatibility in minerals that crystallize from mafic to silicic melts (Mahood and Hildreth, 1983), resulting in enrichment of residual melts formed during extreme fractional crystallization (Webster et al., 1989; Hofstra et al., 2013). Li has thus been used to constrain the patterns and timescales of various magmatic processes. Based on the observations that Li diffuses rapidly in crystals, it has been used to provide information on volcanic processes that happen in minutes to hours,

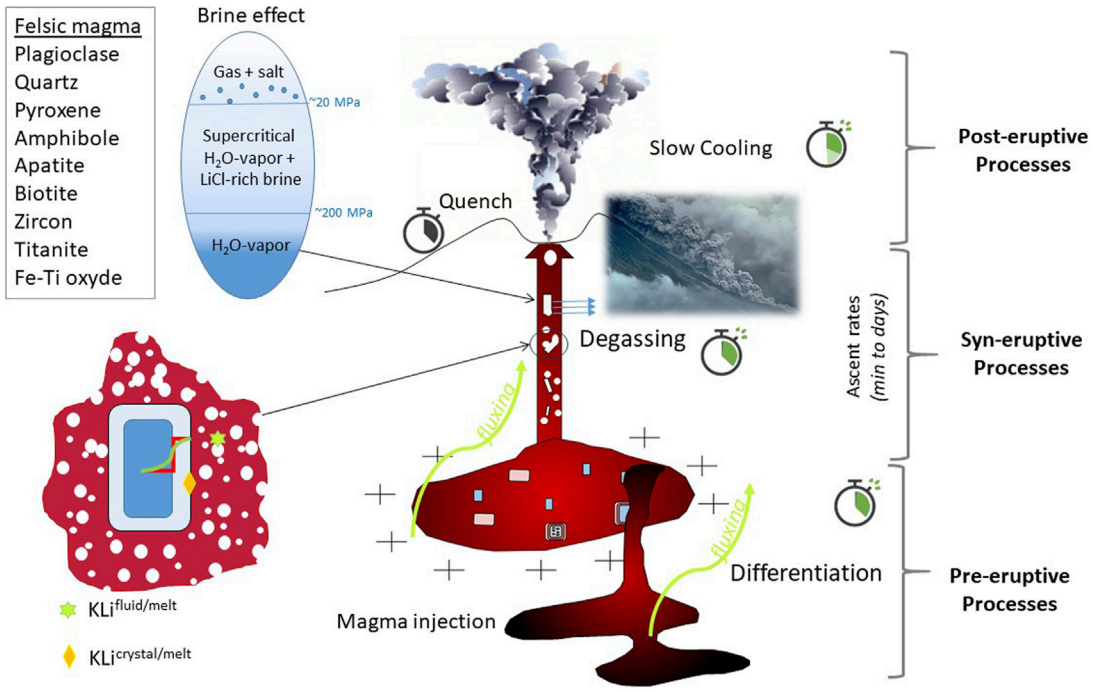


FIGURE 1
Volcanological processes from magma reservoir to eruptive deposits that can be assessed and timed using Li behavior. Magma differentiates in the reservoir and may be perturbed by deep volatile fluxing (green arrows) and new magma injections, which leads to core-to-rim chemical gradients phenocrysts commonly forming in felsic magmas. Li intracrystalline diffusion profiles can be used to assess short (up to days) time lapse between the last injection and eruption, timescales of magma ascent (Neukampf et al., 2021) or cooling (Rubin et al., 2017). Upon ascent, magma outgasses (blue arrow) and the fluid phase may decompose forming brines at low pressure, which has major implications on the Li partition coefficients between fluid and melt ($K_{Li}^{fluid/melt}$) and crystal and melt ($K_{Li}^{crystal/melt}$) (Charlier et al., 2012). Post-eruptive cooling may be responsible of Li mobility, thus being an indicator of cooling rate (Ellis et al., 2018). Post-eruptive Li remobilization, nevertheless, obliterates the pristine distribution of Li between melt and crystal, leading to challenging investigations where using Li as a petrogenetic tracer.

such as crystal growth during magma ascent (Genareau et al., 2010), volatile fluxing and degassing (Berlo et al., 2004; Kent et al., 2007; Vlastélic et al., 2011; Charlier et al., 2012; Giuffrida et al., 2018; Saafeld et al., 2022; Neukampf et al., 2022), and post-eruptive cooling (Gallagher and Elliott, 2009; Ellis et al., 2018). As a result, Li behavior provides information about the conditions and changes that occur during magma storage and ascent (Figure 1). The eruptive dynamics observable at the surface and their explosiveness are dependent on ascent rate and degassing, from eruptive volcanic products Li profiles content in glasses and minerals preserve the information about processes. So, Li appears to be a promising candidate for tracing processes like degassing and fluids in space and time occurring during eruption.

Our present understanding of Li behavior is reviewed here, with a focus on felsic magmas in volcanological settings, where data are still missing. Hereafter, Li diffusion in melts and crystals (feldspar, quartz, pyroxene, amphibole, Fe-Ti oxides, apatite, and zircon), Li partitioning between the crystal, melt, and fluid phases ($H_2O$-rich phase and brines), and Li isotope fractionation are presented. Based on case studies, we show that accurate interpretations of the Li behavior are still debated and we propose future directions for moving forward with the use of Li in volcanological studies.

# 2 Lithium characteristics

## 2.1 Chemistry

Lithium belongs to the alkali metal group. It has a low atomic number (Z = 3) and a small ionic radius of 0.76 Å. Li has two stable isotopes, $^{6}$Li and $^{7}$Li (8% and 92% atomic abundance, respectively), that show one of the largest mass differences (~17%) compared to other stable isotope systems (~10% for $^{10}$B -$^{11}$B and ~12.5% for $^{16}$O -$^{18}$O). Formed at the universe creation by nucleosynthesis following the big-bang, the formation of new Li atoms nowadays is caused by spallation, i.e., by cosmic radiation destruction of atoms heavier than Li such as carbon and oxygen. In crystals, Li often substitutes for Mg (0.72 Å) because both elements have similar ionic radii (Shannon, 1976; Kent and Rossman, 2002). However, in Mg-free or Mg-poor crystal frameworks such as feldspar, Li replaces the main divalent cations at the large octahedral A-site with ions with ionic radii in the range of about 1–1.5 Å (Deubener et al., 1991).

## 2.2 Concentrations and technical challenges

The abundance of Li on Earth is extremely low (about 20–70 ppm in the terrestrial crust, i.e., the 33rd most abundant

**TABLE 1 Bibliographic synthesis of the lithium concentrations in glasses, minerals, and fluid phase, and isotopic ratios.**

| Bulk-rock composition | Phase | $\delta^7$Li (‰) | Concentration (in ppm) | References |
|---|---|---|---|---|
| **Glasses** | | | | |
| Dacite | Bulk | | 5–35 | Kent et al. (2007); Tomascak et al. (2016) |
| | Plagioclase-hosted glass inclusions | | 17–26 | Kent et al. (2007) |
| Topaz rhyolite | Bulk | | ~140 | Webster et al. (1989); Mercer et al. (2015) |
| Macusani rhyolite | Bulk | | >1,000 | London et al. (1988); Pichavant et al. (1988) |
| Rhyolite | Groundmass glasses | | <50 | Berlo et al. (2004) Gurenko et al. (2005); Liu et al. (2006); Cabato et al. (2013); Kent et al. (2007); Balcone-Boissard et al. (2018); Ellis et al. (2018); Neukampf et al. (2019, 2022, 2023) |
| | Plagioclase-hosted glass inclusions | | <50 | Berlo et al. (2004); Gurenko et al. (2005); Liu et al. (2006); Cabato et al. (2013); Kent et al. (2007); Balcone-Boissard et al. (2018); Ellis et al. (2018); Neukampf et al. (2019), Neukampf et al. (2022), Neukampf et al. (2023) |
| | Plagioclase-hosted glass inclusions from Plinian tephra | | 11–397 | Dunbar and Hervig (1992a); Neukampf et al. (2019) |
| | Plagioclase-hosted glass inclusion from ignimbrite | | 15–100 | Dunbar and Hervig (1992a) |
| | Quartz-hosted glass inclusion from plinian tephra | | 17–244 | Dunbar and Hervig (1992a); Neukampf et al. (2019) |
| | Quartz-hosted glass inclusions from ignimbrite | | 19–209 | Dunbar and Hervig (1992a) |
| | Experimental glasses (800°C, 200 MPa, H2O saturated) | | 20–30 | Gion et al. (2022) |
| | Experimental glasses (850°C–1,050°C, 200 MPa, halogen-bearing fluid phase) | | <535 | Iveson et al. (2018), Iveson et al. (2019) |
| **Minerals** | | | | |
| Dacite | Plagioclase | +8 to −5 | 4–25 | Berlo et al. (2004); Bachmann et al. (2005); Cabato et al. (2013); Ellis et al. (2018); Forni et al. (2016), Forni et al. (2018); Neukampf et al. (2019), Neukampf et al. (2023) |
| | Plagioclase | 0 to +5 | 40–50 | Kent et al. (2007) |
| Rhyolite | Quartz | +5 to +8 | 3–25 | Friedrich et al. (2020); Neukampf et al. (2019), Neukampf et al. (2022) |
| | Sanidine | 0 | <5 | Bachmann et al. (2005); Neukampf et al. (2019) |
| | Pyroxene | | <31 | Forni et al. (2016), Forni et al. (2018); Neukampf et al. (2019), Neukampf et al. (2023) |
| | Amphibole | | <30 | Bachmann et al. (2005) |
| | Biotite | | <100 | Forni et al. (2016), Forni et al. (2018); Ellis et al. (2022a) |
| | Zircon | | <120 | Rubin et al. (2017) |
| | Titanite | | <2 | Bachmann et al. (2005) |
| Ore-associated rhyolite | Apatite | | <10 | Duan and Jiang (2018) |
| Granite | Apatite | | ~50 | Li et al. (2022) |
| **Fluid** | | | | |
| Rhyolite | Pure $H_2O$ fluid | | 5–20 | Gion et al. (2022) |
| | Halogen-bearing aqueous fluid | | 4–650 | Iveson et al. (2019) |

element on Earth crust; Aral and Vecchio-Sadus, 2011). Li is considered lithophile and is found in abundance in the silicate layers of the planet. However, the very low contents of Li in volcanic rocks (bulk, melt, and crystals) require the use of high spatial resolution *in-situ* analytical techniques, such as Laser-Ablation Inductively Coupled Plasma Mass Spectrometry (LA-ICPMS; Tomascak et al., 2016) and Secondary Ion Mass spectrometry (SIMS, nano-SIMS or TOF-SIMS; Chaussidon and Robert, 1998; Kasemann et al., 2005; Bell et al., 2009). At comparable spatial resolution, measurement accuracy using LA-ICPMS is generally considered to be lower than using SIMS (Marks et al., 2008), with a spot size of several tens of micrometers (>20 µm; Myers et al., 2019; Neukampf et al., 2019). SIMS and nano-SIMS can quantify Li concentrations and isotope ratios using spots down to 5 µm, enabling analysis of smaller phases (e.g., microlites and melt inclusions), as well as the creation of point-by-point traverses (profiles). TOF-SIMS enables Li to be mapped on a surface, allowing to determine the relative distribution of Li between different phases. To the present day, electronic microprobe (EPMA) is not yet able to measure Li concentrations in glasses or minerals, due to the difficulty of identifying the Li energy peak. However, future developments are expected in the next few years.

We summarize below previous published data on Li contents in bulk felsic magmas, minerals, and glasses (also reported in Table 1).

### 2.2.1 Bulk concentrations

The Li content of the mantle's peridotites from which the magmas derived by partial melting is low, 1.9 ± 0.2 ppm (Ryan and Lagnmuir, 1987). Compared with other rocks, the mantle is low in Li, but due to its large volume it is the most important reservoir on Earth. However, in subduction zones, the Li-enriched slab can metasomatize mantle rocks when dehydrating (Marschall et al., 2017). In felsic lavas, Li typically range ~5–35 ppm (Kent et al., 2007; Tomascak et al., 2016; Ellis et al., 2018; Gion et al., 2022), although specific rhyolites are naturally enriched in Li, with contents up to ~140 ppm in topaz rhyolites (Webster et al., 1989; Mercer et al., 2015) and >1,000 ppm in the Macusani rhyolite (London et al., 1988; Pichavant et al., 1988). Li enrichment in crust may depend on its thickness and the extent of differentiation processes, such as in arc context (Chen et al., 2020).

### 2.2.2 Glass concentrations: residual glass and melt inclusions

Natural rhyolitic glasses and melt inclusions mostly contain less than 50 ppm Li (Berlo et al., 2004; Gurenko et al., 2005; Liu et al., 2006; Cabato et al., 2013; Kent et al., 2007; Balcone-Boissard et al., 2018; Ellis et al., 2018; Neukampf et al., 2019; Neukampf et al., 2022; Neukampf et al., 2023). Rarer still, Li contents higher than 100 ppm (Berlo et al., 2004) and up to ~400 ppm, were also measured (Dunbar and Hervig, 1992a; Dunbar and Hervig, 1992b; Forni et al., 2016; Forni et al., 2018; Neukampf et al., 2019). In some case studies, Li contents in melt inclusions are greater than those found in residual glass (up to a factor 6; Neukampf et al., 2019) while the concentrations of immobile trace elements are identical, suggesting that melt inclusions thus may preserve pre-eruptive Li content in magma. Yet, some melt inclusions may partially re-equilibrate with host-mineral upon degassing (Audétat et al., 2018; Neukampf et al., 2019), so that Li data should be treated with caution.

Aiming at analyzing major and trace elements in low-salinity fluids equilibrated with felsic melts at high pressure and high temperature, Gion et al. (2022) performed experiments at 200 MPa and 800°C in internally-heated pressure vessels, wherein the magmatic fluids were quenched and recovered for analyses by ion chromatography and ICP-MS. Li concentrations in these water-saturated rhyolitic glasses are ~20–30 ppm. Using Li-doped rhyodacitic melts equilibrated with halogen-bearing aqueous fluids, Iveson et al. (2018) and Iveson et al. (2019) performed experiments at 810°C–1,050°C and 60–405 MPa in internally-heated pressure vessels. They analyzed up to 530 ppm Li by ICPMS, thus highlighting that the presence of halogens in the fluids enriches the melt in Li.

### 2.2.3 Mineral concentrations

Li concentrations in natural minerals (plagioclase, quartz, sanidine, pyroxene, amphibole, apatite, titanite, zircon) grown from rhyolitic and granitic melts are typically less than 50 ppm (Berlo et al., 2004; Bachmann et al., 2005; Kent et al., 2007; Cabato et al., 2013; Forni et al., 2016, Forni et al., 2018; Rubin et al., 2017; Duan and Jiang, 2018; Ellis et al., 2018; Neukampf et al., 2019; Neukampf et al., 2022; Neukampf et al., 2023; Friedrich et al., 2020; Li et al., 2022). Yet, Li concentrations up to 120 ppm can be found in biotites and zircons from rhyolitic magmas (Forni et al., 2016; Forni et al., 2018; Ellis et al., 2022a), which then represent the Li-richest minerals in felsic volcanic rocks.

### 2.2.4 Fluid concentrations

Because analyzing Li contents in the fluid phase is technically challenging, data are scarce. Recently, procedures for the direct analysis of quenched, magmatic-hydrothermal fluids recovered from high-pressure and high-temperature experiments have been established using solution ICP-MS (Iveson et al., 2019) or ion chromatography (Gion et al., 2022). Li contents in the fluid phase range from 5–20 ppm at 850°C and 200 MPa (Gion et al., 2022) to 4–650 ppm at similar conditions but in presence of a Cl-bearing fluid phase (Iveson et al., 2019).

## 2.3 Partition coefficients

### 2.3.1 Crystal-melt partition coefficient

Given the low Li concentrations in coexisting melt and crystal phases, the equilibrium constant of Li exchange between such phases can be approximated by the distribution constant between crystal and melt, $K_{Li}^{crystal/melt}$, mostly acquired from natural glass inclusions in their host minerals or from phenocryst rims and their surrounding residual glasses. More rarely, values of the distribution constant were determined from phase equilibrium experiments, mostly performed at atmospheric pressure, temperatures >1,200°C, starting with basaltic compositions (e.g., Bindeman et al., 1998; Aigner-Torres et al., 2007). We summarize below $K_{Li}^{crystal/melt}$ determined from natural and experimentally-produced felsic samples (Table 2).

Plagioclase-rhyolite Li partition coefficients, $K_{Li}^{plag/rhy}$, determined from the natural samples, range from 0.1 to 0.7

**TABLE 2 Bibliographic synthesis of crystal-melt partition coefficients for various minerals in natural and experimental felsic magmas.**

| Phase | Glass composition | P (MPa) | T (°C) | $K_{Li}^{crystal/melt}$ | References |
|---|---|---|---|---|---|
| Natural samples | | | | | |
| Plagioclase | Dacite | 100–150 | ~900 | 0.19–0.28 | Cabato et al. (2013) |
| | | 150 | 840–880 | 0.18–0.22 | Smith et al. (2009) |
| | Rhyolite | 300 | 930–950 | 0.15–0.16 | Brophy et al. (2011) |
| | | 100–200 | 770–856 | 0.1–0.7 | Neukampf et al. (2019)<br>Padilla et Gualda (2016)<br>Charlier et al. (2012) |
| Sanidine | Rhyolite | 100–200 | 770–856 | 0.23–0.32 | Bachmann et al. (2005)<br>Padilla et Gualda (2016)<br>Neukampf et al. (2019) |
| Quartz | Rhyolite | <150 | 770–856 | 0.31–0.58 | Neukampf et al. (2019) |
| Clinopyroxene | Rhyolite | <150 | 770–856 | 0.23–0.32 | Neukampf et al. (2019) |
| Orthopyroxene | Rhyolite | 300 | 930–950 | 0.06–0.09 | Brophy et al. (2011) |
| | | <150 | 770–856 | 0.18–0.22 | Neukampf et al. (2019) |
| Amphibole | Dacite Rhyolite | 150–200 | 700–856 | 0.1–2.0 | Bachmann et al. (2005)<br>Padilla et Gualda (2016)<br>Neukampf et al. (2019) |
| | Rhyolite | 300 | 930–950 | 0.56–0.90 | Brophy et al. (2011) |
| | | 200 | 700–760 | 277 | Padilla et Gualda (2016) |
| Apatite | Rhyolite | 300 | 930–950 | 0.001–0.010 | Brophy et al. (2011) |
| | | 200 | 700–760 | 277 | Padilla et Gualda (2016) |
| | Dacite | 200 | 700–760 | 1–8 | Bachmann et al. (2005)<br>Padilla et Gualda (2016)<br>Bea et al. (1994) |
| | | 200 | 650–750 | 0.8–1.67 | Icenhower and London (1995) |
| Biotite | Dacite | 200 | 700–760 | 1–8 | Bachmann et al. (2005)<br>Padilla et Gualda (2016)<br>Bea et al. (1994) |
| | | 200 | 650–750 | 0.8–1.67 | Icenhower and London (1995) |
| Titanite | Rhyolite | 200 | 700–760 | <0.1–15 | Bachmann et al. (2005)<br>Padilla et Gualda (2016) |
| Magnetite | Rhyolite | <150 | 770–856 | 0.03–0.2 | Neukampf et al. (2019) |
| Experimental samples | | | | | |
| Plagioclase | Fluid-saturated rhyodacite | 150–405 | 810–850 | 0.20–0.28 | Iveson et al. (2018) |
| Quartz | H2O-saturated granite | 300 | 630 | <0.1 | Pichavant (2022) |
| Clinopyroxene | Fluid-saturated rhyodacite | 150–405 | 810–850 | 0.20–0.31 | Iveson et al. (2018) |
| Amphibole | Fluid-saturated rhyodacite | 150–405 | 810–850 | 0.13–0.33 | Iveson et al. (2018) |

P for pressure, T for temperature, and $K_{Li}^{crystal/melt}$ is the crystal-melt partition coefficient.

(Bachmann et al., 2005; Smith et al., 2009; Brophy et al., 2011; Charlier et al., 2012; Cabato et al., 2013; Padilla and Gualda, 2016; Neukampf et al., 2019; Neukampf et al., 2023) (Figure 2A). This agrees with the experimental $K_{Li}^{plag/rhy}$ of 0.2–0.3 determined at 835°C–850°C and 150–360 MPa by Iveson et al. (2019). All $K_{Li}^{plag/melt}$ measured are <1, which demonstrates the incompatibility of Li in plagioclase, resulting from Li preferentially partitioning into the melt. By an experimental study, Coogan et al. (2011) suggested a strong plagioclase composition dependence of Li partitioning between Li-free and Li-bearing plagioclases (melt absent) at

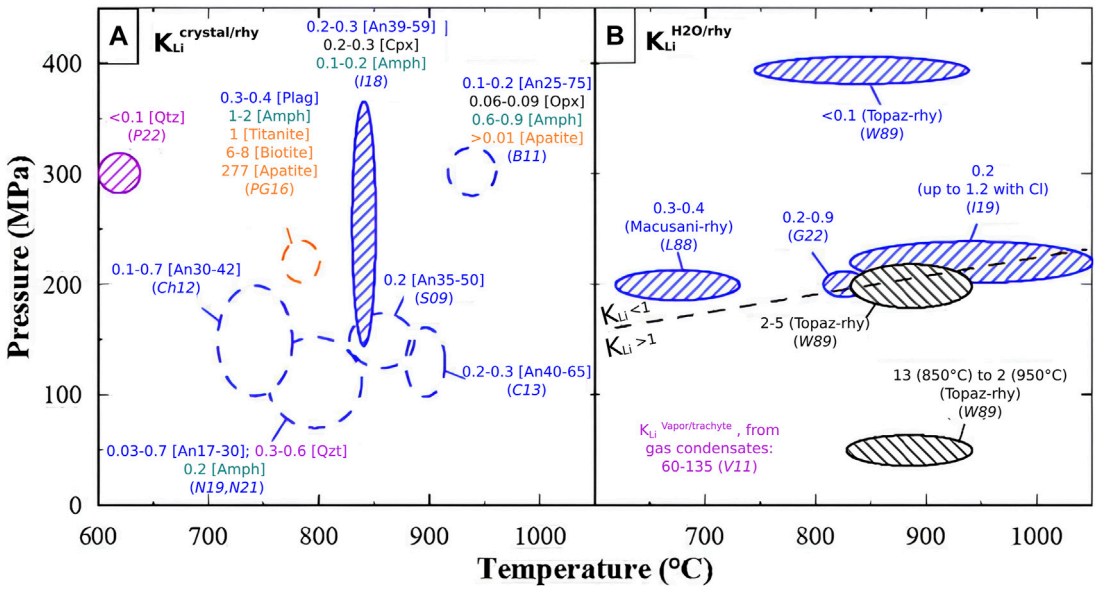


FIGURE 2
Data compilation on Li partitioning between a rhyolitic melt and **(A)** crystals, $K_{Li}^{crystal/melt}$, calculated from crystal-hosted glass inclusions (dashed circles) or phase equilibria (hatched domains); blue for plagioclase (Plag or anorthite molar content, An), purple for quartz (Qtz), green for amphibole (Amph), orange for titanite, biotite, and apatite; data from (**S09**): Smith et al. (2009), (**B11**): Brophy et al. (2011), (**Ch12**): Charlier et al. (2012), (**C13**): Cabato et al. (2013) with the pressure-temperature conditions from Holness et al. (2005), (**PG16**): Padilla and Guada (2016); (**I18**): Iveson et al. (2018) with anorthite contents from Iveson et al. (2017), (**N21**): Neukampf et al. (2021), and (**P22**): Pichavant (2022), and **(B)** a $H_2O$ vapor phase, $K_{Li}^{H2O/melt}$, determined from phase equilibrium experiments; The black dashed line separates $K_{Li}^{fluid/melt} < 1$ from >1; data from (**L88**): London et al. (1988), (**W89**): Webster et al. (1989), (**V11**): Vlastélic et al. (2011) for a partition coefficient measured between gas condensates and a trachytic melt; (**I19**): Iverson et al. (2019), and (**G22**): Gion et al. (2022).

1 atm and 1,000°C, with $K_{Li}$ decreasing by a factor of ~3.5 from $An_{60}$ to $An_{90}$. These melt-absent conditions, however, hardly compare with natural volcanic samples. By an experimental approach using mafic melts, Bindeman et al. (1998) and Bindeman and Davis (2000) concluded to insignificant $K_{Li}$ dependence to plagioclase composition. There are no experimental studies on the temperature dependence of $K_{Li}^{crystal/melt}$, but calculations of trace element partition coefficients, based on the continuum theories of elastic strain and point charges in crystal lattices, consider the effects of temperature, pressure and composition as most important constraints (Blundy and Wood, 2003; Dohmen and Blundy, 2014). The profound effect of pressure and temperature on mineral-melt partitioning can be parameterized in terms of the melting reaction of the trace element component with the same stoichiometry as the host mineral, showing, for example, an increase of the mineral-melt partitioning with increasing pressure (over few GPa; Blundy and Woods, 2003).

Li partition coefficients between other crystals and silicic melts are also mostly <2.0 (quartz: Bachmann et al., 2005; Neukampf et al., 2019; Neukampf et al., 2023; sanidine: Padilla et Gualda, 2016; Neukampf et al., 2019; Neukampf et al., 2023; pyroxene: Brophy et al., 2011; Neukampf et al., 2019; amphibole: Bachmann et al., 2005; Padilla et Gualda, 2016; Neukampf et al., 2019; magnetite: Neukampf et al., 2019; titanite: Bachmann et al., 2005; Padilla et Gualda, 2016; Figure 2A). These natural data agree with those determined experimentally from phase equilibria (quartz: Pichavant, 2022; amphibole: Iveson et al., 2018; pyroxene: Iveson et al., 2018; Brophy et al., 2011; Figure 2A). Yet, higher Li partition coefficients involving the Li-richest minerals have been measured in natural samples (up to 20 in biotite: Bea et al., 1994; Icenhower and London, 1995; Bachmann et al., 2005; Padilla et Gualda, 2016; Ellis et al., 2022a; up to 277 in apatite; Padilla et Gualda, 2016; Figure 2A).

### 2.3.2 Fluid-melt partition coefficient

$K_{Li}^{fluid/melt}$, defined as the ratio of the Li activity in the exsolved fluid phase to that in the melt, has mostly been calculated by mass balance from Li measurements in the bulk and residual glasses or, less frequently, from direct measurements of Li in both phases, the fluid and the glass.

Experimental determinations of $K_{Li}^{H2O/melt}$ are reported in Figure 2B. Gion et al. (2022) reported $K_{Li}^{H2O/rhy}$ from 0.2 to 0.9. Starting from the Li-rich Macusani rhyolites, London et al. (1988) reported $K_{Li}^{H2O/Macusani-rhy}$ of 0.3–0.4 at 200 MPa and 650°C–775°C. Both studies suggest that Li partitions into the rhyolitic melt over the aqueous fluid. Starting with Li-rich topaz-rhyolites, Webster et al. (1989) measured $K_{Li}^{H2O/topaz-rhy}$ from 0.1 to 13 at 770°C–950°C and 50–400 MPa in the presence of aqueous fluids, indicating preferential partition of Li into either melt or vapor, depending on the pressure-temperature conditions. From measurements on natural trachytic pumices and gas condensates, Vlastélic et al. (2011) reported $K_{Li}^{vapor/trachyte}$ from 60 to 135, suggesting that Li strongly partitions into the vapor relative to melt.

Whereas London et al. (1988) found no dependence of $K_{Li}^{H2O/Macusani-rhy}$ on temperatures ranging from 650°C to 775°C at 200 MPa, Webster et al. (1989) found an increase of $K_{Li}^{H2O/topaz-rhy}$ (from 2 to 13) with temperature decreasing from 950°C to 850°C for

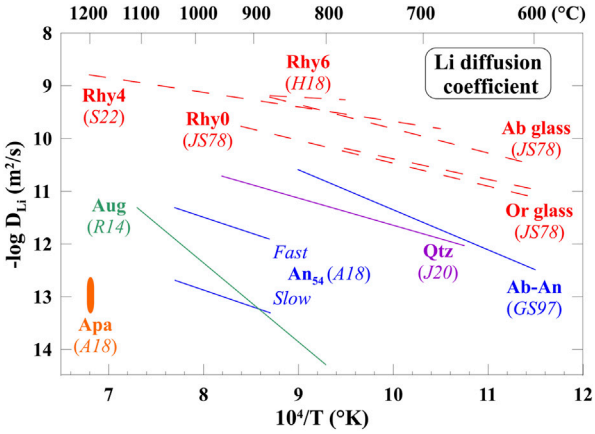


FIGURE 3
Data compilation on Arrhenius relations of Li diffusion in silicic melts (red dashed lines) and plagioclase crystals (blue plain lines). *Rhy0*, *Rhy4*, and *Rhy6* are rhyolitic melts with 0, 4, and 6 wt% $H_2O$, respectively; *Ab glass* and *Or glass* are glasses of albite and orthoclase compositions, respectively; $An_{54}$ denotes a plagioclase composition of 54 mol% anorthite; *Ab-An* corresponds to a plagioclase compositional range from albite to anorthite; *Aug* is for augite and *Qtz* for quartz. Data from (**V52**): Verhoogen (1952), (**JS78**): Jambon and Semet (1978), (**GS97**): Giletti and Shanahan (1997), (**R14**): Richter et al. (2014), (**H18**): Holycross et al. (2018), (**A18**): Audétat et al. (2018), (**J20**): Jollands et al. (2020), (**S22**): Spallanzani et al. (2022).

pressures ≤200 MPa (maximum $K_{Li}^{H2O/topaz\text{-}rhy}$ of 13 at 50 MPa and 850°C). Webster et al. (1989) also suggested a decrease of $K_{Li}^{H2O/topaz\text{-}rhy}$ (from >2 to <0.1) with pressure increasing from 50 to 400 MPa (Figure 2B). These results globally indicate that Li partitions in favor of melt at pressures higher than ~200 MPa. Adding $CO_2$ in the fluid phase significantly decreases the Li partitioning coefficient (Webster et al., 1989) while increasing it with adding halogens (Webster et al., 1989; Iveson et al., 2019). Iveson et al. (2019) concluded that Li is moderately-strongly fluid-immobile at depth and suffers from significant post-eruptive re-equilibration.

## 2.4 Diffusion coefficients

Composition gradients form through elemental or isotopic Li diffusion as a result of disequilibrium processes (changes in temperature, volatile contents, etc.). Li diffusion coefficients ($D_{Li}$) are commonly determined experimentally by re-equilibrating Li-bearing glasses or crystals at a given temperature. In rhyolitic melts, $D_{Li}^{rhy}$ increases from ~$10^{-9.5}$ to $10^{-8.5}$ $m^2/s$ from 700°C to 1,200°C in hydrated rhyolitic melts (Holycross et al., 2018; Spallanzani et al., 2022), and increases from about 0.5 log unit from dry to hydrated rhyolites (Jambon and Semet, 1978; Holycross et al., 2018; Spallanzani et al., 2022) (Figure 3).

In crystals, Li diffuses slower than in melts by more than 1 log unit (Figure 3). Depending on the crystal $D_{Li}$ range from about $10^{-14}$ to $10^{-11}$ $m^2/s$, for temperature between 500°C and 1,250°C (Figure 3). The effect of crystal composition with solid solution such as plagioclase is not clearly established or ruled out. In quartz, Li shows the fastest diffusion coefficient (Jollands et al., 2020). Li diffusivity has also been estimated in apatite, which is a late-stage crystallizing mineral (Audétat et al., 2018).

## 2.5 Isotope fractionation

$^6Li$ and $^7Li$ are today produced by spallogenic reactions, but $^7Li$ was also produced in significant amounts during big-bang nucleosynthesis and during H-burning in stars. The $^6Li/^7Li$ ratio of the solar system is thus explained by a dilution of pure $^7Li$ by spallogenic Li (Chaussidon and Robert, 1998). The isotopic ratio is given as $\delta\,^7Li$:

$$\partial^7 Li = \left( \frac{(^7Li/^6Li)_{sample}}{(^7Li/^6Li)_{standard}} - 1 \right) \times 1000$$

where the standard ($Li_2CO_3$, called L-SVEC) has a $^7Li/^6Li$ ratio of 12.02. Positive values of $\delta^7Li$ express an enrichment in $^7Li$ compared to $^6Li$ (isotopically heavy), whereas negative values of $\delta\,^7Li$ suggest a depletion in $^7Li$ compared to $^6Li$ (isotopically light). Because of the large mass difference between the two isotopes (~17%), equilibrium and kinetic Li isotope fractionation has been reported for a wide range of Earth science processes (Penniston-Dorland et al., 2017). In the past, large scale of fractionation in the upper crust (>80‰ for $\delta^7Li$; Tomascak et al., 2016) make Li an isotopic system of considerable interest in tracing subduction zone processes and crustal recycling (Liu et al., 2020; Teng et al., 2004; Tomascak et al., 2016). Combining Li rapid diffusion in most geologically relevant materials (Tomascak et al., 2016; Holycross et al., 2018) and the large mass difference between $^7Li$ and $^6Li$ explain why kinetic fractionation of Li in magmatic systems is frequent.

Technically, Li isotopes can be analyzed in a variety of ways. The MC-ICPMS allows precise analysis of stable Li isotopes, but only on solutions, which prevents *in situ* measurement in a given phase. Coupled with laser, this technique represents a new and simple means of determining *in situ* isotopic composition in solid phases. SIMS (SIMS, Nano-SIMS, Tof-SIMS) is the technique with the best spatial resolution and sensitivity to efficiently and accurately measure both Li and elemental lithium isotopes.

$\delta^7Li$ ranges from −5 to +16‰ in andesitic to rhyolitic lavas, and from −10 to +20‰ in plutonic rocks such as granites (e.g., Chan et al., 2002; Teng et al., 2004; Ellis et al., 2018) (Figure 4). This variability in the isotopic signal has been attributed to magma sources containing different amounts of recycled material (Elliott et al., 2006; Halama et al., 2008).

In plagioclase, $\delta^7Li$ typically ranges from −10 to +10‰ (Ellis et al., 2018; Neukampf et al., 2019, Neukampf et al., 2021), with rare values as low as −30‰ (Cabato et al., 2013) (Figure 4). The groundmass glasses contain approximately +6 to +8‰ (Neukampf et al., 2019). In granites, fractional crystallization governs Li isotopic behavior and enriches heavier Li isotopes (Yang et al., 2023). In granitic pegmatites, interpreted as the final product of significant fractional crystallization of a peraluminous granitic melt, fluid exsolution during melt-fluid separation may be responsible for significant Li isotopic fractionation in a $H_2O$-poor silica-rich melt (Zhang et al., 2021). During magma degassing, diffusional isotope fractionation may occur because $^6Li$ diffuses faster than $^7Li$ (e.g., Richter et al., 2003; Holycross et al., 2018)

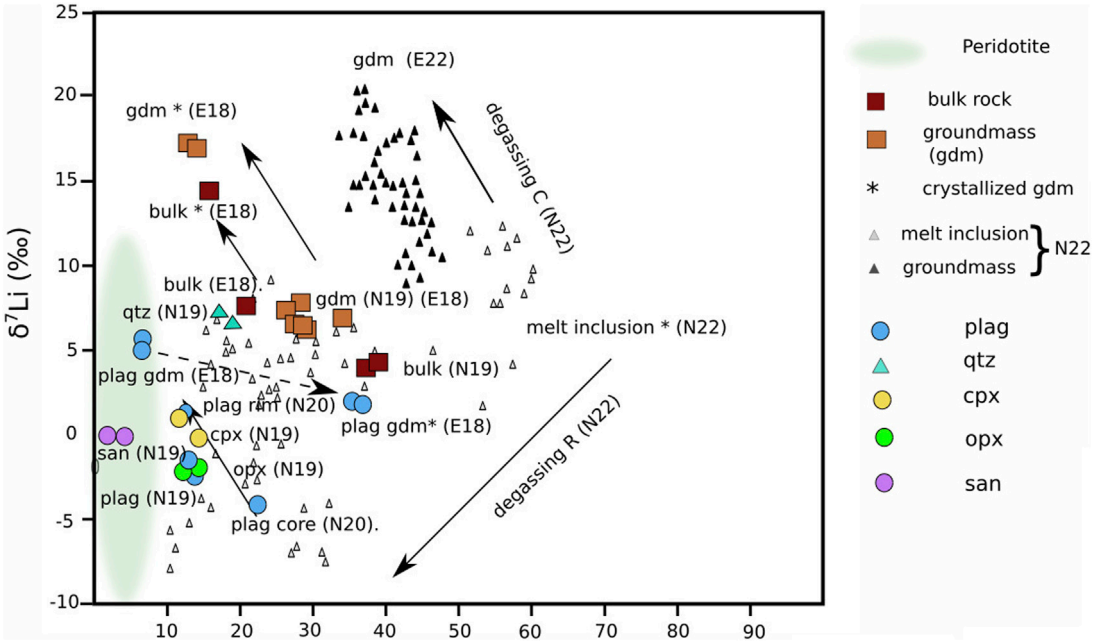


FIGURE 4
Compilation of the $\delta^7$Li data as a function of the Li content for rhyolitic bulk compositions. Data from **(E18)**: Ellis et al. (2018); **(N19)**: Neukampf et al. (2019); **(N20)**: Neukampf et al. (2021); **(N22)**: Neukampf et al. (2022). The legend refers to: bulk: the whole rock; gdm: the groundmass, which more (gdm*) or less (gdm) crystallized. The comparison between bulk peridotite (Ryan and Langmuir, 1987), and rhyolite bulk and glasses show an enrichment of melt during magma differentiation. **N19**: a detailed inventory of Li distribution in a rhyolitic magma coming from Mesa Falls Tuff (Yellowstone), including bulk rocks, groundmass and minerals [plagioclase (plag), quartz (qtz), orthopyroxene (opx), clinopyroxene (cpx), sanidine (san)]. **E18:** Li isotopic and elemental Li distribution in the example of the Tuff of Knob, by comparing bulk rock, groundmass and plagioclases. **E22:** Li elemental and isotopic evolution from Mesa Falls Tuff (as **N19**), in groundmass and melt inclusions in quartz. They discuss various degassing stages: degassing in the reservoir (*degassing R—melt inclusion data*) and in the conduit (*degassing C—groundmass data*) (Neukampf et al., 2022). The solid arrows show the trend linked to magma degassing, where Li partitions preferentially into the vapor phase and consequently depletes the melt and the crystal rims (Ellis et al., 2018; Neukampf et al., 2021). The dashed arrow shows post-eruptive Li movement; for instance, Li enrichment in the plagioclase rims by slow cooling-induced microcrystallization of the groundmass glass (gdm*), with respect to initial glassy groundmass (gdm, Ellis et al., 2018).

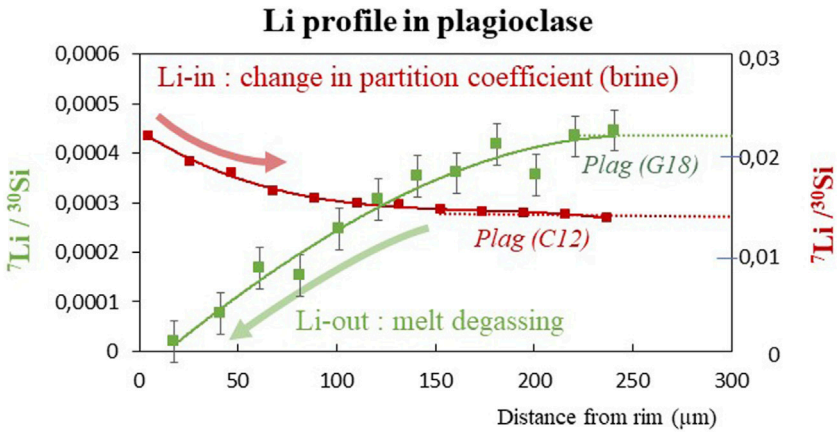


FIGURE 5
Interpretations of contrasted $^7$Li/$^{30}$Si profiles in plagioclases. Core-to-rim Li profiles in plagioclases from the literature showing $^7$Li rim depletion (in green; Giuffrida et al., 2018 (*G18*); left-hand *Y*-axis scale) and $^7$Li rim enrichment [in red; Charlier et al., 2012 (*C12*); right-hand *Y*-axis scale]. Rimward Li depletion is interpreted as open-system degassing that drives Li from the melt into the volatile phase due to $KLi^{fluid/melt} > 1$, consequently draining Li from crystal to melt due to $KLi^{plag/melt} < 1$ (Giuffrida et al., 2018; Neukampf et al., 2023). On the other hand, Li enrichment near the rim is interpreted as Li reentering the crystal in favor of interactions with LiCl-bearing vapors, such as brines, which drastically modify $KLi^{fluid/melt}$ (Kent et al., 2007; Charlier et al., 2012), as described in text.

and $^{7}$Li partitions preferentially into the vapor phase over silicate rocks, particularly at low temperature (e.g., Wunder et al., 2007) and during low-pressure vapor-saturated crystallization (Vlastélic et al., 2011; Watson, 2017). Degassing can create strong isotopic fractionation and extremely light Li compositions, as demonstrated by Watson (2017) who calculated $\delta^{7}$Li as low as −27‰ during decompression-induced bubble growth in a rhyolitic melt. These results agree with the values of $-21 < \delta^{7}\text{Li} < -17$‰ reported by Vlastélic et al. (2011) for degassed pumice samples. By numerical simulation, Luo et al. (2021) demonstrated that diffusional isotope fractionation increases with temperature and from rhyolitic to basaltic melts, and that water slightly weakens the temperature dependence.

# 3 Dilemmas in interpreting Li behavior

Li inventory in volcanic rocks is challenging, because it frequently results from the superimposition of various magmatic (e.g., magma mixing, crystallization, degassing, crystal breakdown, brine exsolution) or external (e.g., hydrothermal alteration, deep vapor fluxing) processes. These processes can either reach thermodynamic equilibrium or induce disequilibrium by diffusion and partitioning preserved in erupted material. As a result, a precise understanding of a volcano's eruptive processes using lithium necessitates careful research into the patterns and timescales of individual processes involving variations in Li content, distribution and isotopic composition. Knowledge of the eruptive behavior of a system, combined with monitoring data such as fumarole analysis, would make it possible to develop an effective petrological monitoring tool. There are several issues with accurate interpretations of the Li behavior, as described below.

## 3.1 Diversity of Li profiles in natural crystals

The composition of major and trace elements in crystals formed from silicate melt is determined by thermodynamic variables (P, T, $fO_2$, $fH_2O$). As a result, minerals are valuable archives of magmatic environments. Minerals frequently show flat profiles in Li concentration (e.g., Cabato et al., 2013), which is consistent with Li high diffusivity ($D_{Li}^{Plag} \sim 10^{-10.5\ to\ -13}$ m$^2$/s at magmatic conditions; Figure 3). Nonetheless, some crystals exhibit heterogeneous Li concentrations or isotopic contents (e.g., Smith and Brown, 1988), indicating disequilibrium as the cause of continuous Li diffusion (Figure 5). For instance, core-to-rim Li profiles in plagioclase phenocrysts either show rimward declines (e.g., Panienka, 2012; Cabato et al., 2013; Giuffrida et al., 2018; Holland et al., 2020; Neukampf et al., 2021; Neukampf et al., 2022), coupled to an almost systematic inverse correlation to $\delta^{7}$Li (Cabato et al., 2013), or Li enrichment towards the rims (Charlier et al., 2012; Panienka, 2012).

Processes invoked to explain core-to-rim decreases of Li and $\delta^{7}$Li involve degassing which drives Li from the melt into the volatile phase due to melt-fluid partitioning in favor of the fluid phase ($KLi^{fluid/melt} > 1$), which in turn drains Li from crystal to melt due to the incompatible nature of Li ($KLi^{plag/melt} < 1$; Cabato et al., 2013; Giuffrida et al., 2018; Neukampf et al., 2023). Li enrichment near the rim of the plagioclase, on the other hand, has been interpreted as an interaction with LiCl-bearing vapors such as brines (Kent et al., 2007; Charlier et al., 2012). Furthermore, during slow cooling, post-eruptive Li diffusion from the residual melt towards the phenocryst rims has been emphasized (Ellis et al., 2018) (Figure 5).

Therefore, interpreting Li gradients in minerals in order to assess the genuine magmatic processes necessitates understanding of how Li partitions between crystal and melt, how the Li isotopic composition evolves with decompression and the presence of complex fluids (such as brine), and whether the Li inventory was modified by post-eruptive cooling. For instance, a thorough study of the degassing process (Charlier et al., 2012; Vlastélic et al., 2011), either magmatic or volatile fluxing, would require to investigate the Li behavior in the fluid phase using $K_{Li}^{fluid/melt}$ (at equilibrium) in the range of conditions of interest, because $K_{Li}^{fluid/melt}$ is dependent on pressure (Webster et al., 1989) and on vapor composition (Webster et al., 1989; Iveson et al., 2018). Similarly, interpreting core-to-rim Li enrichment in minerals in terms of cooling-induced processes (e.g., Gallagher and Elliott, 2009; Ellis et al., 2018) requires the use of $K_{Li}^{crystal/melt}$ and $D_{Li}^{crystal}$ determined for the temperature range of interest.

At the surface Li may or may not degas depending on its behavior at depth (reservoir and conduit), in crystal (see Section 3.2) and respect to the presence of a fluid phase (see Section 3.3).

## 3.2 Timescales retrieved from diffusion modeling

Using Li diffusivity data and isotopic or elemental profiles in crystals has proven useful in resolving timescales of various magmatic processes, such as syn-eruptive magma ascent rates (e.g., Charlier et al., 2012; Giuffrida et al., 2018; Neukampf et al., 2021; Saalfeld et al., 2022), time lapse between a perturbation and the eruption—the perturbation being either vapor fluxing (Kent et al., 2007) or thermal history favoring eruptability (Rubin et al., 2017; Wilson et al., 2017). For instance, Kent et al. (2007) proposed that high Li signature in plagioclase phenocrysts from the 1980 and 2004 climactic eruptions of Mount St Helens volcano (United States), related to vapor transfer and accumulation, occurred within ~1 year before eruption.

Timescales deduced from Li diffusion modelling can be discussed with other geochemical monitoring signals. For instance, Rubin et al. (2017) coupled Li diffusion chronometry in zircons from a rhyolitic magma of Taupo volcano (New Zealand) to U-Th dating of individual zircons to highlight near-solidus long-term crystal storage in a reservoir episodically and locally intruded by small hot magma injections. Yet, such a scenario was questioned by Wilson et al. (2017) based on zircon composition (inappropriateness between the Li concentrations in the natural zircons and the diffusion parameters used for modelling), Li structural distribution in zircon (and possible coupled diffusion mechanisms), and crystal growth rates (modelling requires Li diffusion without crystal growth).

This underscores the need of understanding the conditions driving Li diffusion before constraining timescales of magmatic processes using diffusive chronometry. Of prime relevance is temperature, because diffusivity is strongly temperature

dependent. Indeed, although $D_{Li}$ in silicic melts seems to only vary by 1 log unit between dry and hydrated conditions or between rhyolite and plagioclase melts compositions, $D_{Li}$ in plagioclase crystals vary by more than 1.5 log units (Figure 3), highlighting the need for more studies to explain these differences.

## 3.3 Partition coefficients determined from melt inclusions

$K_{Li}^{crystal/melt}$ is mostly determined from melt inclusions trapped in minerals. After entrapment and before quench, melt can be modified by volatile loss and crystallization during magma decompression and cooling or conversely by dissolution of the host crystal (Rose-Koga et al., 2021 for a review). As a result, the chemical compositions of the melt and the host crystal can be altered, with the principal outcome being that the Li inventory in the glass and its host crystal no longer reflects crystal-melt equilibrium and obfuscates the initial entrapment conditions. Therefore, studies using $K_{Li}^{crystal/melt}$ determined from glass inclusions necessitate careful inspection of the glass and its host mineral (Neukampf et al., 2019; Rose-Koga et al., 2021). Such studies on melt inclusions also highlight the feedback of other diffusing species, such as H or Cu, acting as modifiers of pristine Li concentration by Li–H diffusional exchange during late stage degassing upon eruption (Jollands et al., 2020; Neukampf et al., 2022). FTIR or cathodoluminescence mapping may help illuminating heterogeneous distribution in crystal and/or melt inclusions. The primary Li content of melt inclusions may also be modified naturally by re-equilibration with a Li-rich brine in the reservoir (Kent et al., 2007; Preece et al., 2014), as detailed below.

## 3.4 The brine effects

Fluids in magma plumbing systems may occur in a supercritical state or as mixtures of low-density vapour (gas), higher density liquids (e.g., brines), and precipitated solutes, depending on the pressure–temperature conditions of fluid release and initial chemical composition of the fluid. Brines consist of aqueous liquids enriched in alkalis (e.g., Na) and halogens (e.g., Cl), likely forming a few kilometers beneath active or dormant volcanoes (Afanasyev et al., 2018), which are of particular importance in concentrating Li. Indeed, an alkali-rich silicate melt in equilibrium with a vapour phase at high pressure (>200 MPa) shows immiscibility at subsolvus conditions (<210 MPa at 1,000°C; Chou, 1987, Anderko and Pitzer, 1993; Driesner and Heinrich, 2007), resulting in a $H_2O$-rich vapour phase and a Cl-rich brine, as indicated by the NaCl-$H_2O$ phase diagram. This non-ideal fluid behaviour is responsible of a buffering effect on melt Cl concentration (Gibb's phase rule; Lowenstern, 1994; Balcone-Boissard et al., 2018) but also of changes of Li partitioning at subsolvus conditions (Charlier et al., 2012).

The brine effect, and more precisely the fluid/vapor component, has been highlighted by a Li excess in the rims of quartz and feldspars from a Taupo rhyolitic eruption (Charlier et al., 2012). According to the authors, bubble formation concentrates Li and Cl in the fluid phase, followed by demixing into a supercritical $H_2O$-rich vapour phase and a subcritical brine as the solvus is crossed upon decompression (Sourirajan and Kennedy, 1962; Chou, 1987). At pressure ~20 MPa, the two-fluid phase equilibrium is disrupted: the brine crystallizes into a solid phase and the vapor changes from a supercritical fluid to a gas. This change is crucial for Li, because it is modifying LiCl partitioning: the LiCl of the vapor phase is hydrolysed by high-temperature gases and Li re-enters the silicate melt and the crystals as LiOH species whereas Cl is degassed as HCl acid (Charlier et al., 2012).

As a result, Li can be used to trace the magma's degassing mode, with depleted melts and crystal rims resulting from open-system degassing in which Li partitioned preferentially in the fluid phase and Li-enriched crystal rims resulting from closed-system degassing in the presence of brines at low pressure, where Li partitioned back into the melt. Despite the magmatic-hydrothermal transition's critical role in Li concentration, the change in partitioning when melt and magmatic fluid coexist is poorly understood (Ellis et al., 2022b). In particular, in case $K_{Li}^{fluid/melt/crystal}$ would drastically vary as a function of pressure and fluid composition, alternative explanations could be proposed to account for Li enrichment at crystal rims.

# 4 Perspectives

The aforementioned dilemmas and recommendations highlight the need for further research in order to better interpret Li variations in natural volcanic products and have a chance to use Li as a petrological monitoring tool for active volcanoes in the future.

- Li diffusion in minerals seems to vary by more than 4 orders of magnitude depending on the crystal species and temperature, which needs further investigations. The choice of the mineral in which Li gradients are studied is also important, since tracing Li in apatite that is a late-stage crystallizing phase in silicic melts could bring simpler information than recorded in crystals with a long and complex crystallization history (Miles et al., 2013). Li distribution into the atomic structure of the minerals is certainly of major interest for determining $D_{Li}$, but also for testing Li coupled diffusion with other trace elements.
- Crystal-melt Li partition coefficients have mostly been determined from melt inclusions, for which the equilibration conditions are not well defined. To help interpreting Li gradients in minerals, experimental data need to be extended to larger domains of temperature (for which the $K_{Li}^{crystal/melt}$ dependence has not been demonstrated), pressure (for which there is a lack of data at < 200 MPa), and mineral species (e.g., scarce data for accessory minerals). Systematic experiments have to be run to check the crystal composition dependence of the $K_{Li}^{crystal/melt}$. A greater understanding of $K_{Li}^{crystal/melt}$ may also aid in determining the economic potential of volcanic deposits, particularly those of rhyolitic composition (Benson et al., 2017). Although it is beyond the scope of this study, the Li behavior in mafic compositions would be fascinating to investigate in terms of the effect of Fe and S (redox) on $K_{Li}^{crystal/melt}$.
- The Li isotopic signatures in rhyolitic systems and their minerals are very scattered ($\delta^7$Li from −15 to +20‰),

which likely involve the contribution of processes other than degassing. As a result, the parameters controlling $\delta^7$Li in minerals and glasses still need to be constrained to fully use $\delta^7$Li as a tracer of processes and to constrain their timescales. Among these processes, Li isotopic heterogeneity generated during post-eruptive cooling is crucial because it can alter the pristine magmatic information (Ellis et al., 2018).

- Fluid-melt Li partition coefficients involving a pure $H_2O$ or $H_2O$-$CO_2$ fluids are scarce and mostly concern Li-rich rhyolites (e.g., macusani rhyolite or topaz-rhyolite), which strengthens the need of experimental work using "common" rhyolitic melts. Also, the $K_{Li}^{fluid/melt}$ dependence to pressure (suggested by Webster et al., 1989) has to be confirmed, particularly the transition from values >1 (at low pressure) to <1 (at high pressure), because the consequence of Li preferentially partitioning either in the vapor phase or in the melt is a key point to trace the degassing process. The addition of $CO_2$ in the aqueous phase seems to increase Li partitioning into the fluid phase (Webster et al., 1989), but needs systematic confirmation. Continuing research on $K_{Li}^{fluid/melt}$ is also important because on the medium to long term, Li extraction from magmatic fluids can become a hot topic.
- Brines have a significant impact on Li distribution between the fluid, melt, and crystal phase, requiring that interpretations of Li gradients in minerals are supported by well-known fluid-melt partition coefficients in presence of brines. To this aim, phase-equilibrium experiments spanning a range of halogen fluid compositions and performed at low pressures (where supercritical fluids demix into brines) are necessary. This is a pre-requisite step to hope to 1-day link surficial Li-bearing fumaroles to deep degassing processes (as proposed for $^{210}$Pb by Berlo et al., 2004) and use Li as a petrological monitoring tool for active volcanoes.
- Technical developments must be encouraged in order to progress in greater analytical resolutions for always lower Li concentrations (few ppm), smaller (i.e., microlite or experimentally-grown) crystals, and difficult fluid phase investigations. Overcoming technical challenges with trace-element contents, spatial resolution, and *in-situ* measurements opens up new research options for shedding light on magma degassing history and timelines of diffusive processes in natural magmas using complicated Li profiles.

## Author contributions

All authors listed have made a substantial, direct, and intellectual contribution to the work and approved it for publication.

## Funding

This study benefitted from financial support from the French CNRS-INSU_TelluS program (MD), the ANR V-CARE (ANR-18-CE03-0010; G. Boudon), and the LABEX VOLTAIRE project (ANR-10-LABX-100-01; B. Scaillet).

## Acknowledgments

The authors thank M. Pichavant, F. Costa, and B. Dubacq for helpful discussions, the reviewers MM and RM for very helpful and constructive comments, and SM as Guest Editor and V. Acocella as Field Chief Editor for careful editorial handling.

## Conflict of interest

The authors declare that the research was conducted in the absence of any commercial or financial relationships that could be construed as a potential conflict of interest.

## Publisher's note



## References

Afanasyev, A., Blundy, J. D., Melnik, O., and Sparks, S. R. (2018). Formation of magmatic brine lenses via focussed fluid-flow beneath volcanoes. *Earth Planet. Sci. Lett.* 486, 119–128. doi:10.1016/j.epsl.2018.01.013

Aigner-Torres, M., Blundy, J., Ulmer, P., and Pettke, T. (2007). Laser ablation ICPMS study of trace element partitioning between plagioclase and basaltic melts: an experimental approach. *Contrib. Mineral. Petrol.* 153 (6), 647–667. doi:10.1007/s00410-006-0168-2

Anderko, A., and Pitzer, K. S. (1993). Equation-of-state representation of phase equilibria and volumetric properties of the system NaCl-H2O above 573 K. *Geochim. Cosmochim. Acta* 57 (8), 1657–1680. doi:10.1016/0016-7037(93)90105-6

Aral, H., and Vecchio-Sadus, M. (2011). "Lithium: environmental pollution and health effects," in *Encyclopedia of environmental health*. Editor J. O. Nriagu (Amsterdam, Netherlands: Elsevier), 499–508. doi:10.1016/B978-0-444-52272-6.00531-6

Audétat, A., Zhang, L., and Ni, H. (2018). Copper and Li diffusion in plagioclase, pyroxenes, olivine and apatite, and consequences for the composition of melt inclusions. *Geochim. Cosmochim. Acta* 243, 99–115. doi:10.1016/j.gca.2018.09.016

Bachmann, O., Dungan, M. A., and Bussy, F. (2005). Insights into shallow magmatic processes in large silicic magma bodies: the trace element record in the fish canyon magma body, colorado. *Contrib. Mineral. Petrol.* 149 (3), 338–349. doi:10.1007/s00410-005-0653-z

Balcone-Boissard, H., Boudon, G., Blundy, J. D., Martel, C., Brooker, R. A., Deloule, E., et al. (2018). Deep pre-eruptive storage of silicic magmas feeding Plinian and dome-forming eruptions of central and northern Dominica (Lesser Antilles) inferred from volatile contents of melt inclusions. *Contrib. Mineral. Petrol.* 173, 101. doi:10.1007/s00410-018-1528-4

Bea, F., Pereira, M. D., and Stroh, A. (1994). Mineral/leucosome trace-element partitioning in a peraluminous migmatite (a laser ablation-ICP-MS study). *Chem. Geol.* 117 (1–4), 291–312. doi:10.1016/0009-2541(94)90133-3

Bell, A. W., Deutsch, E. W., Au, C. E., Kearney, R. E., Beavis, R., Sechi, S., et al. (2009). A HUPO test sample study reveals common problems in mass spectrometry–based proteomics. *Nat. Methods* 6, 423–430. doi:10.1038/nmeth.1333

Benson, T. R., Coble, M. A., Rytuba, J. J., and Mahood, G. A. (2017). Lithium enrichment in intracontinental rhyolite magmas leads to Li deposits in caldera basins. *Nat. Commun.* 8, 270. doi:10.1038/s41467-017-00234-y

Berlo, K., Blundy, J., Turner, S., Cashman, K., Hawkesworth, C., and Black, S. (2004). Geochemical precursors to volcanic activity at Mount St. Helens, USA. *Science* 306, 1167–1169. doi:10.1126/science.1103869

Berzelius, J. J. (1817). *Lärbok i kemien. 6 vols*. Stockholm: Nordström.

Bindeman, I. N., Davis, A. M., and Drake, M. J. (1998). Ion microprobe study of plagioclase-basalt partition experiments at natural concentration levels of trace elements. *Geochim. Cosmochim. Acta* 62 (7), 1175–1193. doi:10.1016/s0016-7037(98)00047-7

Bindeman, I. N., and Davis, A. M. (2000). Trace element partitioning between plagioclase and melt: investigation of dopant influence on partition behavior. *Geochim. Cosmochim. Acta* 64 (16), 2863–2878. doi:10.1016/S0016-7037(00)00389-6

Blundy, J., and Wood, B. (2003). Partitioning of trace elements between crystals and melts. *Earth Planet. Sci. Lett.* 210, 383–397. doi:10.1016/s0012-821x(03)00129-8

Brophy, J. G., Ota, T., Kunihro, T., Tsujimori, T., and Nakamura, E. (2011). *In situ* ion-microprobe determination of trace element partition coefficients for hornblende, plagioclase, orthopyroxene, and apatite in equilibrium with natural rhyolitic glass, Little Glass Mountain Rhyolite, California. *Am. Mineral.* 96, 1838–1850. doi:10.2138/am.2011.3857

Cabato, J., Altherr, R., Ludwig, T., and Meyer, H.-P. (2013). Li, Be, B concentrations and δ7Li values in plagioclase phenocrysts of dacites from Nea Kameni (Santorini, Greece). *Contrib. Mineral. Petrol.* 165, 1135–1154. doi:10.1007/s00410-013-0851-z

Chan, L. H., Leeman, W. P., and You, C.-F. (2002). Lithium isotopic composition of central American volcanic arc lavas: implications for modification of subarc mantle by slab-derived fluids: correction. *Chem. Geol.* 182, 293–300. doi:10.1016/s0009-2541(01)00298-4

Charlier, B. L. A., Morgan, D. J., Wilson, C. J. N., Wooden, J. L., Allan, A. S. R., and Baker, J. A. (2012). Lithium concentration gradients in feldspar and quartz record the final minutes of magma ascent in an explosive supereruption. *Earth Planet. Sci. Lett.* 319-320, 218–227. doi:10.1016/j.epsl.2011.12.016

Chaussidon, M., and Robert, F. (1998). 7Li/6Li and 11B/10B variations in chondrules from the Semarkona unequilibrated chondrite. *Earth Planet. Sci. Lett.* 164 (3–4), 577–589. doi:10.1016/S0012-821X(98)00250-7

Chen, C., Lee, C. T. A., Tang, M., Biddle, K., and Sun, W. (2020). Lithium systematics in global arc magmas and the importance of crustal thickening for lithium enrichment. *Nat. Commun.* 11, 5313. doi:10.1038/s41467-020-19106-z

Chou, I.-M. (1987). Phase relations in the system NaCl-KCl-H2O. III: solubilities of halite in vapor-saturated liquids above 445°c and redetermination of phase equilibrium properties in the system nacl-h2o to 1000°c and 1500 bars. *Geochim. Cosmochim. Acta* 51 (7), 1965–1975. doi:10.1016/0016-7037(87)90185-2

Coogan, L. A. (2011). Preliminary experimental determination of the partitioning of lithium between plagioclase crystals of different anorthite contents. *Lithos* 125 (1-2), 711–715. doi:10.1016/j.lithos.2011.03.016

Deubener, J., Sternitzke, M., and Müller, G. (1991). Feldspars $MAlSi_3O_8$ (M = H, Li, Ag) synthesized by low-temperature ion exchange. *Am. Mineral.* 76, 1620–1627.

Dohmen, R., and Blundy, J. (2014). A predictive thermodynamic model for element partitioning between plagioclase and melt as a function of pressure, temperature and composition. *Am. J. Sci.* 314, 1319–1372. doi:10.2475/09.2014.04

Driesner, T., and Heinrich, C. A. (2007). The system H2O–NaCl. Part I: correlation formulae for phase relations in temperature–pressure–composition space from 0 to 1000°c, 0 to 5000 bar, and 0 to 1 xnacl. *Geochim. Cosmochim. Acta* 71 (20), 4880–4901. doi:10.1016/j.gca.2006.01.033

Duan, D.-F., and Jiang, S.-Y. (2018). Using apatite to discriminate synchronous ore-associated and barren granitoid rocks: A case study from the edong metallogenic district, south China. *Lithos* 310–311, 369–380. doi:10.1016/j.lithos.2018.04.022

Dunbar, N. W., and Hervig, R. L. (1992a). Petrogenesis and volatile stratigraphy of the bishop tuff: evidence from melt inclusion analysis. *J. Geophys. Res. Solid Earth* 97 (B11), 15129–15150. doi:10.1029/92jb00764

Dunbar, N. W., and Hervig, R. L. (1992b). Volatile and trace element composition of melt inclusions from the lower bandelier tuff: implications for magma chamber processes and eruptive style. *J. Geophys. Res. Solid Earth* 97 (B11), 15151–15170. doi:10.1029/92jb01340

Elliott, T. R., Thomas, A., Jeffcoat, A., and Niu, Y. (2006). Lithium isotope evidence for subduction-enriched mantle in the source of mid-ocean-ridge basalts. *Nature* 443 (7111), 565–568. doi:10.1038/nature05144

Ellis, B. S., Neukampf, J., Bachmann, O., Harris, C., Forni, F., Magna, T., et al. (2022a). Biotite as a recorder of an exsolved Li-rich volatile phase in upper crustal silicic magma reservoirs. *Geology* 50, 481–485. doi:10.1130/G49484.1

Ellis, B. S., Szymanowski, D., Harris, C., Tollan, P. M. E., Neukampf, J., Guillong, M., et al. (2022b). Evaluating the potential of rhyolitic glass as a lithium source for brine deposits. *Econ. Geol.* 117 (1), 91–105. doi:10.5382/econgeo.4866

Ellis, B. S., Szymanowski, D., Magna, T., Neukampf, J., Dohmen, R., Bachmann, O., et al. (2018). Post-eruptive mobility of lithium in volcanic rocks. *Nat. Commun.* 9, 3228. doi:10.1038/s41467-018-05688-2

Forni, F., Bachmann, O., Mollo, S., De Astis, G., Gelman, S. E., and Ellis, B. S. (2016). The origin of a zoned ignimbrite: insights into the campanian ignimbrite magma chamber (campi flegrei, italy). *Earth Planet. Sci. Lett.* 449, 259–271. doi:10.1016/j.epsl.2016.06.003

Forni, F., Petricca, E., Bachmann, O., Mollo, S., De Astis, G., and Piochi, M. (2018). The role of magma mixing/mingling and cumulate melting in the Neapolitan Yellow Tuff caldera-forming eruption (Campi Flegrei, southern Italy). *Contrib. Mineral. Petrol.* 173, 45. doi:10.1007/s00410-018-1471-4

Friedrich, A. M., Laurent, O., Heinrich, C. A., and Bachmann, O. (2020). Melt and fluid evolution in an upper-crustal magma reservoir, preserved by inclusions in juvenile clasts from the Kos Plateau Tuff, Aegean Arc, Greece. *Geochim. Cosmochim. Acta* 280, 237–262. doi:10.1016/j.gca.2020.03.038

Gallagher, K., and Elliott, T. (2009). Fractionation of lithium isotopes in magmatic systems as a natural consequence of cooling. *Earth Planet. Sci. Lett.* 278, 286–296. doi:10.1016/j.epsl.2008.12.009

Genareau, K., and Clarke, A. B. (2010). *In situ* measurements of plagioclase growth using SIMS depth profiles of $^{7}Li/^{30}Si$: A means to acquire crystallization rates during short duration decompression events. *Am. Mineral.* 95, 592–601. doi:10.2138/am.2010.3292

Giletti, B. J., and Shanahan, T. M. (1997). Alkali diffusion in plagioclase feldspar. *Chem. Geol.* 139, 3–20. doi:10.1016/S0009-2541(97)00026-0

Gion, A. M., Gaillard, F., Freslon, N., Erdmann, S., and Di Carlo, I. (2022). A method for the direct analysis of quenched, magmatic-hydrothermal fluids recovered from high-pressure, high-temperature experiments. *Chem. Geol.* 609, 121061. doi:10.1016/j.chemgeo.2022.121061

Giuffrida, M., Viccaro, L., and Ottolini, M. (2018). Ultrafast syn-eruptive degassing and ascent trigger high-energy basic eruptions. *Sci. Rep.* 8, 147. doi:10.1038/s41598-017-18580-8

Gurenko, A. A., Trumbull, R. B., Thomas, R., and Lindsay, J. M. (2005). A melt inclusion record of volatiles, trace elements and Li-B isotope variations in a single magma system from the Plat Pays Volcanic Complex, Dominica, Lesser Antilles. *J. Petrol.* 46, 2495–2526. doi:10.1093/petrology/egi063

Halama, R., McDonough, W. F., Rudnick, R. L., and Bell, K. (2008). Tracking the lithium isotopic evolution of the mantle using carbonatites. *Earth Planet. Sci. Lett.* 265 (3–4), 726–742. doi:10.1016/j.epsl.2007.11.007

Hofstra, A. H., Todorov, T. I., Mercer, C. N., Adams, D. T., and Marsh, E. E. (2013). Silicate melt inclusion evidence for extreme pre-eruptive enrichment and post-eruptive depletion of lithium in silicic volcanic rocks of the western United States: implications for the origin of lithium-rich brines. *Econ. Geol.* 105, 1691–1701. doi:10.2113/econgeo.108.7.1691

Holness, M. B., Martin, V. M., and Pyle, D. M. (2005). Information about open-system magma chambers derived from textures in magmatic enclaves: the kameni islands, santorini, greece. *Geol. Mag.* 142, 637–649. doi:10.1017/s0016756805001172

Holycross, M., Watson, E., Richter, F., and Villeneuve, J. (2018). Diffusive fractionation of Li isotopes in wet, silicic melts. *Geochem. Perspect. Lett.* 6, 39–42. doi:10.7185/geochemlet.1807

Huang, F., Lundstrom, C. C., and McDonough, W. F. (2006). Effect of melt structure on trace-element partitioning between clinopyroxene and silicic, alkaline, aluminous melts. *Am. Mineral.* 91, 1385–1400. doi:10.2138/am.2006.1909

Icenhower, J., and London, D. (1995). An experimental study of element partitioning among biotite, muscovite, and coexisting peraluminous silicic melt at 200 MPa (H2O). *Am. Mineral.* 80 (11–12), 1229–1251. doi:10.2138/am-1995-11-1213

IEA (2021). *The role of critical minerals in clean energy transitions*. Paris: IEA. Available at: https://www.iea.org/reports/the-role-of-critical-minerals-in-clean-energy-transitions (License: CC BY 4.0.

Iveson, A. A., Rowe, M. C., Webster, J. D., and Neill, O. K. (2018). Amphibole-clinopyroxene- and plagioclase-melt partitioning of trace and economic metals in halogen-bearing rhyodacitic melts. *J. Petrol.* 59 (8), 1579–1604. doi:10.1093/petrology/egy072

Iveson, A. A., Webster, J. D., Rowe, M. C., and Neill, O. K. (2019). Fluid-melt trace-element partitioning behaviour between evolved melts and aqueous fluids: experimental constraints on the magmatic-hydrothermal transport of metals. *Chem. Geol.* 516, 18–41. doi:10.1016/j.chemgeo.2019.03.029

Iveson, A. A., Webster, J. D., Rowe, M. C., and Neill, O. K. (2017). Major element and halogen (F, Cl) mineral–melt–fluid partitioning in hydrous rhyodacitic melts at shallow crustal conditions. *J. Petrol.* 58, 2465–2492. doi:10.1093/petrology/egy011

Jambon, A., and Semet, M. P. (1978). Lithium diffusion in silicate glasses of albite, orthoclase, and obsidian composition: an ion-microprobe determination. *Earth Planet. Sci. Lett.* 37, 445–450. doi:10.1016/0012-821x(78)90060-2

Jollands, M. C., Ellis, B., Tollan, P. M. E., and Müntener, O. (2020). An eruption chronometer based on experimentally determined H-Li and H-Na diffusion in quartz applied to the Bishop Tuff. *Earth Planet. Sci. Lett.* 551, 116560. doi:10.1016/j.epsl.2020.116560

Kasemann, S. A., Jeffcoate, A. B., and Elliott, T. (2005). Lithium isotope composition of basalt glass reference material. *Mater.* Anal. Chem. 77 (16), 5251–5257. doi:10.1021/ac048178h

Kent, A. J. R., Blundy, J., Cashman, K. V., Cooper, K. M., Donnelly, C., Pallister, J. S., et al. (2007). Vapor transfer prior to the october 2004 eruption of Mount St. Helens, Washington. *Geology* 35, 231–234. doi:10.1130/g22809a.1

Kent, A. J. R., and Rossman, G. R. (2002). Hydrogen, lithium, and boron in mantle-derived olivine: the role of coupled substitutions. *Am. Mineral.* 87 (10), 1432–1436. doi:10.2138/am-2002-1020

Li, J., Chen, S-Y., and Zhao, Y-H. (2022). Trace elements in apatite from gejiu Sn polymetallic district: implications for petrogenesis, metallogenesis and exploration. *Ore Geol. Rev.* 145, 104880. doi:10.1016/j.oregeorev.2022.104880

Liu, H., Xiao, Y., Sun, H., Tong, F., Heuser, A., Churikova, T., et al. (2020). Trace elements and Li isotope compositions across the kamchatka arc: constraints on slab-derived fluid sources. J. Geophys. Res. *Solid Earth* 125 (5). doi:10.1029/2019JB019237

Liu, Y., Anderson, A. T., Wilson, C. J. N., Davis, A. M., and Steele, I. M. (2006). Mixing and differentiation in the oruanui rhyolitic magma, Taupo, New Zealand: evidence from volatiles and trace elements in melt inclusions. *Contrib. Mineral. Petrol.* 151, 71–87. doi:10.1007/s00410-005-0046-3

London, D., Hervig, R. L., and Morgan, G. B. (1988). Melt-vapor solubilities and elemental partitioning in peraluminous granite-pegmatite systems: experimental results with macusani glass at 200 mpa. *Contrib. Mineral. Petrol.* 99, 360–373. doi:10.1007/bf00375368

Lowenstern, J. B. (1994). Dissolved volatile concentrations in an ore-forming magma. *Geology* 22 (10), 893. doi:10.1130/0091-7613(1994)022<0893:DVCIAO>2.3.CO;2

Luo, H., Karki, B. B., Ghosh, D. B., and Bao, H. (2021). Deep neural network potentials for diffusional lithium isotope fractionation in silicate melts. *Geochim. Cosmochim. Acta* 303, 38–50. doi:10.1016/j.gca.2021.03.031

Mahood, G. A., and Hildreth, W. (1983). Large partition coefficients for trace elements in high-silica rhyolites. *Geochim. Cosmochim. Acta* 47, 11–30. doi:10.1016/0016-7037(83)90087-x

Marks, M. A. W., Rudnick, R. L., Ludwig, T., Marschall, H., Zack, T., Halama, R., et al. (2008). Sodic pyroxene and sodic amphibole as potential reference materials for *in situ* lithium isotope determinations by SIMS. *Geostand. Geoanalytical Res.* 32, 295–310. doi:10.1111/j.1751-908X.2008.00895.x

Marschall, H. R., Wanless, D., Shimizu, N., Pogge von Strandmann, P., Elliot, T., and Monteleone, B. (2017). The boron and lithium isotopic composition of mid-ocean ridge basalts and the mantle. *Geochim. Cosmochim. Acta* 207, 102–138. doi:10.1016/j.gca.2017.03.028

Mercer, C. N., Hofstra, A. H., Todorov, T. I., Roberge, J., Burgisser, A., Adams, D. T., et al. (2015). Pre-eruptive conditions of the hideaway park topaz rhyolite: insights into metal source and evolution of magma parental to the henderson porphyry molybdenum deposit, colorado. *J. Petrol.* 56, 645–679. doi:10.1093/petrology/egv010

Miles, A. J., Graham, C., Hawkesworth, C. J., Gillespie, M. R., and Hinton, R. (2013). Evidence for distinct stages of magma history recorded by the compositions of accessory apatite and zircon. *Contrib. Mineral. Petrol.* 166, 1–19. doi:10.1007/s00410-013-0862-9

Munk, L. A., Hynek, S. A., Bradley, D. C., Boutt, D., Labey, K., and Jochens, H. (2016). Lithium brines: A global perspective. *Soc. Econ. Geol.* Rev. Econ. Geol. 18, 339–365.

Myers, M. L., Wallace, P. J., and Wilson, C. J. N. (2019). Inferring magma ascent timescales and reconstructing conduit processes in explosive rhyolitic eruptions using diffusive losses of hydrogen from melt inclusions. *J. Volcanol. Geotherm. Res.* 369, 95–112. doi:10.1016/j.jvolgeores.2018.11.009

Neukampf, J., Ellis, B. S., Laurent, O., Steinmann, L. K., Ubide, T., Oeser, M., et al. (2021). Time scales of syneruptive volatile loss in silicic magmas quantified by Li isotopes. *Geology* 49, 125–129. doi:10.1130/G47764.1

Neukampf, J., Ellis, B. S., Magna, T., Laurent, O., and Bachmann, O. (2019). Partitioning and isotopic fractionation of lithium in mineral phases of hot, dry rhyolites: the case of the mesa falls tuff, yellowstone. *Chem. Geol.* 506, 175–186. doi:10.1016/j.chemgeo.2018.12.031

Neukampf, J., Ellis, B. S., Magna, T., Laurent, O., and Marrocchi, Y. (2023). Partitioning and isotopic fractionation of Li between mineral phases and alkaline to calc-alkaline melts of explosive and effusive eruptions. *Chem. Geol.* 636, 121628. doi:10.1016/j.chemgeo.2023.121628

Neukampf, J., Laurent, O., Tollan, P., Bouvier, A.-S., Magna, T., Ulmer, P., et al. (2022). Degassing from magma reservoir to eruption in silicic systems: the li elemental and isotopic record from rhyolitic melt inclusions and host quartz in a yellowstone rhyolite. *Geochim. Cosmochim. Acta* 326, 56–76. doi:10.1016/j.gca.2022.03.037

Padilla, A., and Gualda, G. A. R. (2016). Crystal-melt elemental partitioning in silicic magmatic systems: an example from the peach spring tuff high-silica rhyolite, southwest usa. *Chem. Geol.* 440, 326–344. doi:10.1016/j.chemgeo.2016.07.004

Panienka, S. (2012). *PhD, Fakultät für Chemie und Geowissenschaften*.The concentration of lithium in plagioclase crystals of the minoan tephra, (santorini, Greece).

Penniston-Dorland, S., Liu, X.-M., and Rudnick, R. L. (2017). Lithium isotope geochemistry. *Rev. Mineral. Geochem.* 82, 165–217. doi:10.2138/rmg.2017.82.6

Pichavant, M. (2022). Experimental crystallization of the beauvoir granite as a model for the evolution of variscan rare metal magmas. *J. Petrol.* 63. doi:10.1093/petrology/egac120

Pichavant, M., Kontak, D. J., Briqueu, L., Valencia Herrera, J., and Clark, A. H. (1988). The Miocene-Pliocene Macusani Volcanics, SE Peru; II. Geochemistry and origin of a felsic peraluminous magma. *Contrib. Mineral. Petrol.* 100, 325–338. doi:10.1007/bf00379742

Preece, K., Gertisser, R., BarclayBerlo, J. K., Herd, R. A., and Edinburgh Ion Microprobe Facility, (2014). Pre- and syn-eruptive degassing and crystallisation processes of the 2010 and 2006 eruptions of Merapi volcano, Indonesia. *Contrib. Mineral. Petrol* 168, 1061. doi:10.1007/s00410-014-1061-z

Richter, F. M., Davis, A. M., DePaolo, D. J., and Watson, E. B. (2003). Isotope fractionation by chemical diffusion between molten basalt and rhyolite. *Geochim. Cosmochim. Acta* 67, 3905–3923. doi:10.1016/s0016-7037(03)00174-1

Richter, F., Watson, B., Chaussidon, M., Mendybaev, R., and Ruscitto, D. (2014). Lithium isotope fractionation by diffusion in minerals. Part 1: pyroxenes. *Geochim. Cosmochim. Acta* 126, 352–370. doi:10.1016/j.gca.2013.11.008

Rose-Koga, E., Bouvier, A. S., Gaetani, G., Wallace, P., Allison, C., Andrys, J., et al. (2021). Silicate melt inclusions in the new millennium: A review of recommended practices for preparation, analysis, and data presentation. *Chem. Geol.* 570 (5), 120145. doi:10.1016/j.chemgeo.2021.120145

Rubin, A. E., Cooper, K. M., Till, C. B., Kent, A. J. R., Costa, F., Bose, M., et al. (2017). Rapid cooling and cold storage ina silicic magma reservoir recorded in individual crystals. *Science* 356, 1154–1156. doi:10.1126/science.aam8720

Ryan, J. G., and Langmuir, C. H. (1987). The systematics of lithium abundances in young volcanic rocks. *Geochim. Cosmochim. Acta* 51 (6), 1727–1741. doi:10.1016/0016-7037(87)90351-6

Saalfeld, M. A., Myers, M. L., deGraffenried, R., Shea, T., and Waelkens, C. M. (2022). On the rise: using reentrants to extract magma ascent rates in the bandelier tuff caldera complex, new mexico, usa. *Bull. Volcanol.* 84, 4. doi:10.1007/s00445-021-01518-4

Schuessler, J. A., Schoenberg, R., and Sigmarsson, O. (2009). Iron and lithium isotope systematics of the Hekla volcano, Iceland - evidence for Fe isotope fractionation during magma differentiation. *Chem. Geol.* 258 (1-2), 78–91. doi:10.1016/j.chemgeo.2008.06.021

Shannon, R. D. (1976). Revised effective ionic radii and systematic studies of interatomic distances in halides and chalcogenides. *Acta Crystallogr.* A32, 751–767. doi:10.1107/s0567739476001551

Smith, J. V., and Brown, W. L. (1988). *Feldspar minerals*, 1. Cham: Springer-Verlag.

Smith, V. C., Blundy, J. D., and Arce, J. L. (2009). A temporal record of magma accumulation and evolution beneath Nevado de Toluca, Mexico, preserved in plagioclase phenocrysts. *J. Petrol.* 50, 405–426. doi:10.1093/petrology/egp005

Sourirajan, S., and Kennedy, G. C. (1962). The system H 2 O-NaCl at elevated temperatures and pressures. *Am. J. Sci.* 260 (2), 115–141. doi:10.2475/ajs.260.2.115

Spallanzani, R., Koga, K. T., Cichy, S. B., Wiedenbeck, M., Schmidt, B. C., Oelze, M., et al. (2022). Lithium and boron diffusivity and isotopic fractionation in hydrated rhyolitic melts. *Contrib. Mineral. Petrol.* 177, 74. doi:10.1007/s00410-022-01937-2

Teng, F.-Z., McDonough, W. F., Rudnick, R. L., Dalpé, C., Tomascak, P. B., Chappell, B. W., et al. (2004). Lithium isotopic composition and concentration of the upper continental crust. *Geochim. Cosmochim. Acta* 68 (20), 4167–4178. doi:10.1016/j.gca.2004.03.031

Tomascak, P. B., Magna, T., and Dohmen, R. (2016). *Advances in lithium isotope geochemistry*. Cham, Switzerland: Springer International Publishing, 195.

Verhoogen, J. (1952). Ionic diffusion and electrical conductivity in quartz. *Am. Mineral.* 37, 637–655.

Vlastélic, I., Staudacher, T., Bachèlery, P., Télouk, P., Neuville, D., and Benbakkar, M. (2011). Lithium isotope fractionation during magma degassing: constraints from silicic differentiates and natural gas condensates from piton de la fournaise volcano (réunion island). *Chem. Geol.* 284, 26–34. doi:10.1016/j.chemgeo.2011.02.002

Watson, E. B. (2017). Diffusive fractionation of volatiles and their isotopes during bubble growth in magmas. *Contrib. Mineral. Petrol.* 172, 61. doi:10.1007/s00410-017-1384-7

Webster, J. D., Holloway, J. R., and Hervig, R. L. (1989). Partitioning of lithophile trace elements between $H_2O$ and $H_2O+CO_2$ fluids and topaz rhyolite melts. *Econ. Geol. Bull. Soc. Econ. Geol.* 84, 116–134. doi:10.2113/gsecongeo.84.1.116

Wilson, C. J. N., Morgan, D. J., Charlier, B. L. A., and Barker, S. J. (2017). Comment on "Rapid cooling and cold storage in a silicic magma reservoir recorded in individual crystals". *Science* 358 (6370), eaap8429. doi:10.1126/science.aap8429

Wunder, B., Meixner, A., Romer, R. L., Feenstra, A., Schettler, G., and Heinrich, W. (2007). Lithium isotope fractionation between Li-bearing staurolite, Li-mica and aqueous fluids: an experimental study. *Chem. Geol.* 238, 277–290. doi:10.1016/j.chemgeo.2006.12.001

Yang, J.-H., Chen, H., Zhou, M.-F., Hu, R.-Z., and Williams-Jones, A. E. W. (2023). Lithium isotope fractionation during intensive felsic magmatic differentiation. *Geochem. Geophys. Geosys.* 24 (4), e2022GC010771. doi:10.1029/2022GC010771

Zhang, H., Tian, S., Wang, D., Li, X., Liu, T., Zhang, Y., et al. (2021). Lithium isotope behavior during magmatic differentiation and fluid exsolution in the Jiajika granite–pegmatite deposit, Sichuan, China. *Ore Geol. Rev.* 134, 104139. doi:10.1016/j.oregeorev.2021.104139